2008 IEEE International Conference on
Robotics and Automation
Pasadena, CA, USA, May 19-23, 2008

Asymptotic Stability of Dynamic Bipedal Gait with Constraint on Impact Posture

Fumihiko Asano and Zhi-Wei Luo

Abstract— **This paper studies the efficiency and asymptotic stability of a dynamic bipedal gait with a constraint on the impact posture. First, we generate a gait by using tracking control to achieve the desired trajectory of the hip-joint angle, and show that there is a trade-off between efficiency and robustness through a numerical simulation. Second, we investigate the asymptotic stability of the gait from the mechanical energy balance viewpoint, and discuss the importance of the control input properties. Furthermore, we point out that there is a feedback in mechanical energy in the discrete walking system, and it is difficult to detect a stable 2-period gait.**

I. INTRODUCTION

Detection of limit cycle stability is a basic problem in research on robotic bipedal locomotion. Dynamic walkers, especially passive-dynamic walkers [1], that generate limit cycles with impacts have been the subject of this sort of study, but their nonlinearity including impulsive effects is very complicated and is not thoroughly understood yet.

Several approaches to detect limit cycle stability have been proposed, and they use certain techniques to simplify the walking system. Among them, the constraint on impact posture is a key factor for the stability of dynamic walking [2][3], and the constraint on restored mechanical energy guarantees a stable gait. We showed that these two constraints asymptotically stabilized dynamic gaits through the same stability mechanism as in a rimless wheel and clarified how gait stability can be guaranteed [4].

Based on observations, this paper studies the asymptotic stability of dynamic bipedal gaits that only have constraint on impact posture. It introduces a planar underactuated biped model with semicircular feet and a torso, which has 2-D.O.F. and one active joint. Both constraint conditions on the impact posture and restored mechanical energy are needed to guarantee the asymptotic stability of the gait. The robot this paper considers, however, can achieve only one constraint condition of them due to the underactuation, and it takes the constraint on impact posture. The restored mechanical energy then changes with respect to the initial conditions and control input. In this case, the features of the restored mechanical energy with respect to the control input must be numerically examined. Through numerical studies, we show how the dynamic bipedal gait changes with respect to the torso's physical parameters. We also discuss the asymptotic stability of the dynamic gait and feedback structure of the mechanical energy inherent to the walking system.

F. Asano and Z.W. Luo are with the Bio-Mimetic Control Research Center, RIKEN, 463-0003 Nagoya, Japan {asano,luoz}@bmc.riken.jp

Z.W. Luo is also with the Department of Computer Science and Systems Engineering, Graduate School of Engineering, Kobe University luo@gold.kobe-u.ac.jp

II. DYNAMIC GAIT GENERATION WITH CONSTRAINT ON IMPACT POSTURE

A. Model of underactuated biped with torso

This paper deals with a planar underactuated biped model with semicircular feet and a torso as shown in Fig. 1. A bisecting hip mechanism (BHM) [5] is used to stabilize the torso passively in an upright pose. Through the synergistic effect of BHM, we can efficiently generate a dynamic bipedal gait without having to maintain the torso's posture actively. Semicircular feet are also very effective for generating an efficient dynamic gait [6][7]. Two joint torques between each leg and torso can be exerted. Let $\boldsymbol{\theta} = \begin{bmatrix}\theta_1 & \theta_2 & \theta_3\end{bmatrix}^{\mathrm{T}}$ be the generalized coordinate vector; the dynamic equation of the biped model is then

$$\boldsymbol{M}(\boldsymbol{\theta})\ddot{\boldsymbol{\theta}} + \boldsymbol{h}(\boldsymbol{\theta}, \dot{\boldsymbol{\theta}}) = \boldsymbol{S}\boldsymbol{u} + \boldsymbol{J}_H^{\mathrm{T}}\lambda_H, \tag{1}$$

where

$$\boldsymbol{S}\boldsymbol{u} = \begin{bmatrix} 1 & 0 \\ 0 & 1 \\ -1 & -1 \end{bmatrix} \begin{bmatrix} u_1 \\ u_2 \end{bmatrix}, \tag{2}$$

and $\boldsymbol{J}_H^{\mathrm{T}}\lambda_H \in \mathbb{R}^3$ denotes the constraint force of the BHM. The geometric relation between the torso and legs according to the BHM is given by

$$\theta_3 = \frac{\theta_1 + \theta_2}{2} + \psi, \tag{3}$$

where ψ [rad] is the offset angle of the torso. We will choose it to be zero and won't investigate its effect. The time derivative of Eq. (3) is

$$\dot{\theta}_3 = \frac{\dot{\theta}_1 + \dot{\theta}_2}{2}. \tag{4}$$

This can be simply rearranged as

$$\boldsymbol{J}_H\dot{\boldsymbol{\theta}} = 0,\ \boldsymbol{J}_H = \begin{bmatrix}1 & 1 & -2\end{bmatrix}. \tag{5}$$

This leads to $\boldsymbol{J}_H\ddot{\boldsymbol{\theta}} = 0$, and by substituting this into Eq. (1) and eliminating λ_H, we obtain

$$\lambda_H = -X_H(\boldsymbol{\theta})^{-1}\boldsymbol{J}_H\boldsymbol{M}(\boldsymbol{\theta})^{-1}\left(\boldsymbol{S}\boldsymbol{u} - \boldsymbol{h}(\boldsymbol{\theta}, \dot{\boldsymbol{\theta}})\right), \tag{6}$$

$$X_H(\boldsymbol{\theta}) = \boldsymbol{J}_H\boldsymbol{M}(\boldsymbol{\theta})^{-1}\boldsymbol{J}_H^{\mathrm{T}}. \tag{7}$$

By substituting Eqs. (6) and (7) into Eq. (1), we can further simplify the robot's dynamic equation to

$$\boldsymbol{M}(\boldsymbol{\theta})\ddot{\boldsymbol{\theta}} = \boldsymbol{Y}_H(\boldsymbol{\theta})\left(\boldsymbol{S}\boldsymbol{u} - \boldsymbol{h}(\boldsymbol{\theta}, \dot{\boldsymbol{\theta}})\right), \tag{8}$$

where

$$\boldsymbol{Y}_H(\boldsymbol{\theta}) = \boldsymbol{I}_3 - X_H(\boldsymbol{\theta})^{-1}\boldsymbol{J}_H^{\mathrm{T}}\boldsymbol{J}_H\boldsymbol{M}(\boldsymbol{\theta})^{-1}. \tag{9}$$

978-1-4244-1647-9/08/$25.00 ©2008 IEEE.

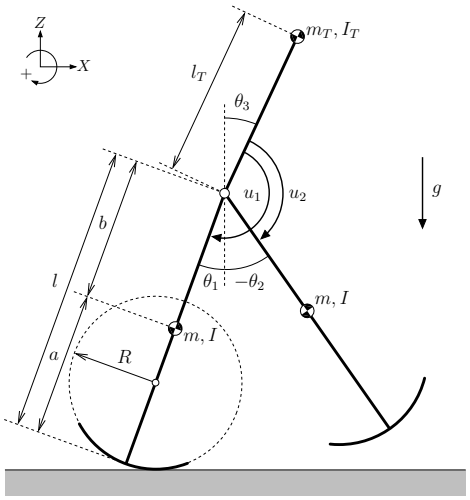

Fig. 1. Model of planar underactuated biped robot with semicircular feet and torso

Please see [8] for further details. The heel-strike is modeled as an inelastic collision and is described in the next section.

B. Dynamic gait generation

We first synthesize a desired trajectory for the hip-joint angle. Considering smooth motion of the hip-joint, we introduce the following fifth-order time-dependent function.

$$\theta_{H\mathrm{d}}(t) = \begin{cases} a_5 t^5 + a_4 t^4 + a_3 t^3 + a_0 & (0 \le t < T_{\mathrm{set}}) \\ \theta_H^* & (t \ge T_{\mathrm{set}}) \end{cases}$$

The coefficients, a_i, are determined so that they satisfy the following boundary conditions:

$$\ddot{\theta}_{H\mathrm{d}}(0) = 0,\ \dot{\theta}_{H\mathrm{d}}(0) = 0,\ \theta_{H\mathrm{d}}(0) = -\theta_H^*,$$
$$\ddot{\theta}_{H\mathrm{d}}(T_{\mathrm{set}}) = 0,\ \dot{\theta}_{H\mathrm{d}}(T_{\mathrm{set}}) = 0, \theta_{H\mathrm{d}}(T_{\mathrm{set}}) = \theta_H^*,$$

and they are given by

$$\begin{bmatrix} a_5 \\ a_4 \\ a_3 \end{bmatrix} = \begin{bmatrix} T_{\mathrm{set}}^5 & T_{\mathrm{set}}^4 & T_{\mathrm{set}}^3 \\ 5T_{\mathrm{set}}^4 & 4T_{\mathrm{set}}^3 & 3T_{\mathrm{set}}^2 \\ 20T_{\mathrm{set}}^3 & 12T_{\mathrm{set}}^2 & 6T_{\mathrm{set}} \end{bmatrix}^{-1} \begin{bmatrix} 2\theta_H^* \\ 0 \\ 0 \end{bmatrix}, \quad (10)$$

and $a_0 = -\theta_H^*$. The desired settling time, T_{set}, is chosen empirically, and we assume that the settling-time condition is always satisfied. After the settling time, the hip-joint angle is kept constant, θ_H^*, and the constraint control on the impact posture is achieved. We simply call the generated gait constrained compass gait.

We now synthesize the output following control by using the hip-joint torque. We choose θ_H as the system's control output; i.e., $\theta_H = \begin{bmatrix} 1 & -1 \end{bmatrix} \boldsymbol{S}^{\mathrm{T}} \boldsymbol{\theta}$, and its second-order derivative with respect to time is

$$\begin{aligned} \ddot{\theta}_H &= \begin{bmatrix} 1 & -1 \end{bmatrix} \boldsymbol{S}^{\mathrm{T}} \ddot{\boldsymbol{\theta}} \\ &= \begin{bmatrix} 1 & -1 \end{bmatrix} \boldsymbol{S}^{\mathrm{T}} \boldsymbol{M}^{-1} \boldsymbol{Y}_H \left(\begin{bmatrix} 1 \\ 0 \\ -1 \end{bmatrix} u_1 - \boldsymbol{h} \right) \\ &=: A u_1 - B, \end{aligned} \quad (11)$$

where

$$A = \begin{bmatrix} 1 & -1 \end{bmatrix} \boldsymbol{S}^{\mathrm{T}} \boldsymbol{M}^{-1} \boldsymbol{Y}_H \begin{bmatrix} 1 \\ 0 \\ -1 \end{bmatrix}, B = \begin{bmatrix} 1 & -1 \end{bmatrix} \boldsymbol{S}^{\mathrm{T}} \boldsymbol{M}^{-1} \boldsymbol{Y}_H \boldsymbol{h}.$$

Then we can consider the following trajectory tracking control input:

$$u_1 = A^{-1} (\bar{u} + B), \quad (12)$$
$$\bar{u} = \ddot{\theta}_{H\mathrm{d}} + k_{\mathrm{d}} \left(\dot{\theta}_{H\mathrm{d}} - \dot{\theta}_H \right) + k_{\mathrm{p}} (\theta_{H\mathrm{d}} - \theta_H), \quad (13)$$

where k_{p} and k_{d} are the PD gains.

Fig. 2 shows the simulation results for a constrained compass gait with the physical parameters as in Table I. The energy efficiency is much worse than that of underactuated virtual passive dynamic walking [8]. The specific resistance is 0.1066 [-]. This is caused by the negative input power due to the tracking control (See Fig. 2 (e)). The mechanical energy must be monotonically restored by the control input to achieve high energy-efficiency, unlike in Fig. 2 (d). However, the robustness of the dynamic gait is much better than one without desired trajectories. The torso length, l_T, can be set very long. Fig. 3 shows the stick diagram for one cycle of motion for a constrained compass gait. We can see from this figure that the long torso is passively stabilized to remain upright through the effect of the BHM [5][8].

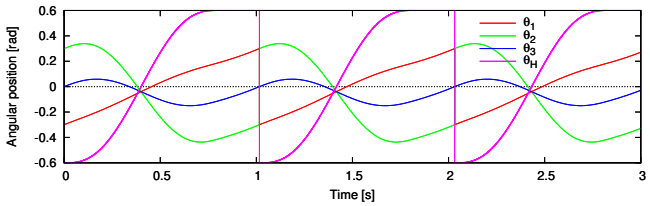

(a) Angular position

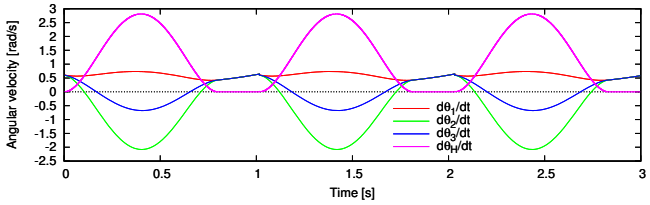

(b) Angular velocity

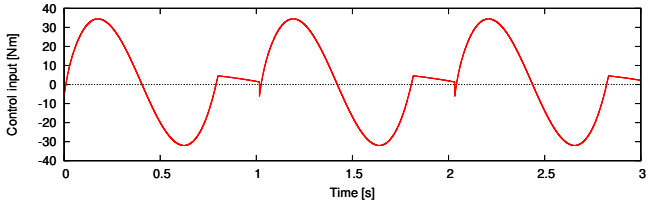

(c) Control input

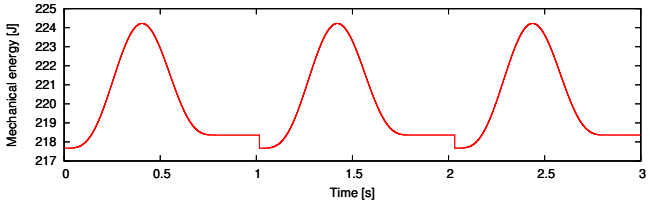

(d) Mechanical energy

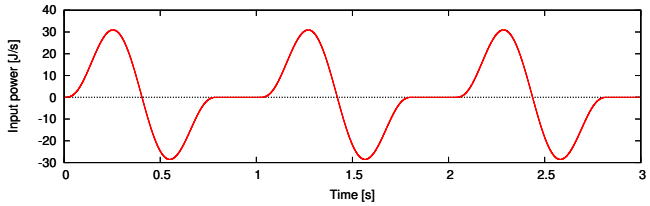

(e) Input power

Fig. 2. Simulation results for constrained compass gait with upper body

TABLE I

PARAMETERS OF BIPED WALKING SYSTEM

m	5.0	kg
m_T	10.0	kg
a	0.50	m
b	0.50	m
$l\ (=a+b)$	1.00	m
l_T	0.70	m
I	0.001	kg·m^2
I_T	0.001	kg·m^2

R	0.30	m
θ_H^*	0.60	rad
ψ	0.00	rad
k_d	100	s^{-1}
k_p	2500	s^{-2}
T_set	0.80	s

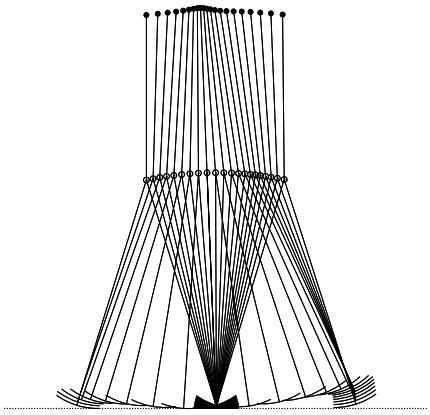

Fig. 3. Stick diagram of steady walking pattern

III. ENERGY LOSS COEFFICIENT

The heel-strike is modeled as an inelastic collision. We introduce the extended coordinate vector, $\boldsymbol{q} \in \mathbb{R}^6$, and the model then becomes

$$\bar{\boldsymbol{M}}(\boldsymbol{q})\dot{\boldsymbol{q}}^+ = \bar{\boldsymbol{M}}(\boldsymbol{q})\dot{\boldsymbol{q}}^- - \boldsymbol{J}_I(\boldsymbol{q})^\mathrm{T}\boldsymbol{\lambda}_I, \tag{14}$$

$$\boldsymbol{J}_I(\boldsymbol{q})\dot{\boldsymbol{q}}^+ = \boldsymbol{0}_{7\times 1}, \tag{15}$$

where $\bar{\boldsymbol{M}} \in \mathbb{R}^{9\times 9}$ and $\boldsymbol{J}_I \in \mathbb{R}^{7\times 9}$. $\boldsymbol{\lambda}_I \in \mathbb{R}^7$ means the impact force on the robot. The details are omitted. Following Eqs. (14) and (15), we obtain the post-impact velocity as

$$\begin{aligned}\dot{\boldsymbol{q}}^+ &= \left(\boldsymbol{I}_9 - \bar{\boldsymbol{M}}^{-1}\boldsymbol{J}_I^\mathrm{T}\left(\boldsymbol{J}_I\bar{\boldsymbol{M}}^{-1}\boldsymbol{J}_I^\mathrm{T}\right)^{-1}\boldsymbol{J}_I\right)\dot{\boldsymbol{q}}^- \\ &=: \boldsymbol{Y}(\boldsymbol{q})\dot{\boldsymbol{q}}^-. \end{aligned}\tag{16}$$

The relation $\dot{\boldsymbol{q}}^- = \boldsymbol{H}(\boldsymbol{q})\dot{\boldsymbol{\theta}}^-$ also holds, where

$$\boldsymbol{H}(\boldsymbol{q}) = \begin{bmatrix} R & 0 & 0 \\ 0 & 0 & 0 \\ 1 & 0 & 0 \\ R+(l-R)\cos\frac{\theta_H^*}{2} & -(l-R)\cos\frac{\theta_H^*}{2} & 0 \\ -(l-R)\sin\frac{\theta_H^*}{2} & -(l-R)\sin\frac{\theta_H^*}{2} & 0 \\ 0 & 1 & 0 \\ R+(l-R)\cos\frac{\theta_H^*}{2} & 0 & 0 \\ -(l-R)\sin\frac{\theta_H^*}{2} & 0 & 0 \\ 0 & 0 & 1 \end{bmatrix}, \tag{17}$$

and this is a function matrix only of θ_H^*. On the other hand, the constraint control of the impact posture leads to the following relation:

$$\dot{\boldsymbol{q}}^- = \boldsymbol{H}(\theta_H^*)\begin{bmatrix}1\\1\\1\end{bmatrix}\dot{\theta}_1^-. \tag{18}$$

By substituting this into Eq. (16) and considering the relation between $\dot{\boldsymbol{\theta}}^+$ and $\dot{\boldsymbol{q}}^+$, we finally obtain

$$\dot{\boldsymbol{\theta}}^+ = \begin{bmatrix}0&0&0&0&0&1&0&0&0\\0&0&1&0&0&0&0&0&0\\0&0&0&0&0&0&0&0&1\end{bmatrix}\boldsymbol{Y}\boldsymbol{H}\begin{bmatrix}1\\1\\1\end{bmatrix}\dot{\theta}_1^- =: \boldsymbol{\xi}\dot{\theta}_1^-. \tag{19}$$

The kinetic energy just after impact is then given by

$$K^+ = \frac{1}{2}\boldsymbol{\xi}^\mathrm{T}\boldsymbol{M}(-\theta_H^*)\boldsymbol{\xi}\left(\dot{\theta}_1^-\right)^2 =: \frac{1}{2}\bar{M}^+\left(\dot{\theta}_1^-\right)^2, \tag{20}$$

and that just before impact on the other hand is

$$K^- = \frac{1}{2}\begin{bmatrix}1\\1\\1\end{bmatrix}^\mathrm{T}\boldsymbol{M}(\theta_H^*)\begin{bmatrix}1\\1\\1\end{bmatrix}\left(\dot{\theta}_1^-\right)^2 =: \frac{1}{2}\bar{M}^-\left(\dot{\theta}_1^-\right)^2. \tag{21}$$

Because of $\boldsymbol{M}(\theta_H^*) = \boldsymbol{M}(-\theta_H^*)$, energy loss coefficient, ε, becomes

$$\varepsilon := \frac{K^+}{K^-} = \frac{\bar{M}^+}{\bar{M}^-}, \tag{22}$$

and depends only on θ_H^*. The constraint control of the impact posture not only reduces the system's D.O.F. [2][3] it also keeps the energy loss coefficient constant.

Fig. 4 plots ε with respect to torso length, l_T, and torso mass, m_T. ε monotonically increases as both parameters increase. The reason is as follows. In such cases, as shown in Fig. 5, the CoM rises and the relative hip-joint angle of its equivalent biped model with mass-less legs closes. This decreases the energy dissipation [7]; i.e., ε increases.

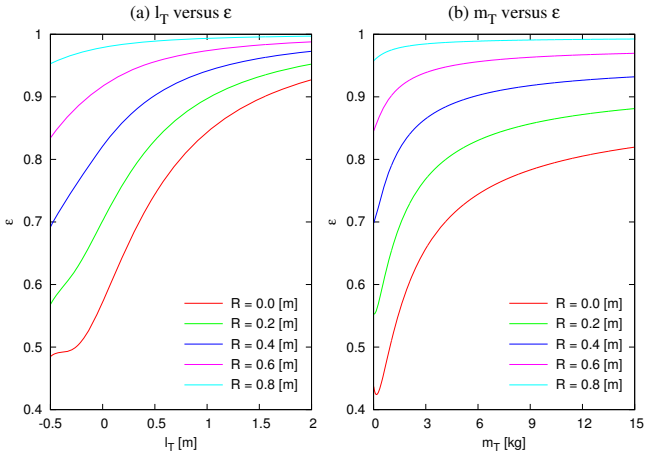

Fig. 4. Plots of ε with respect to parameters of upper body for five values of R

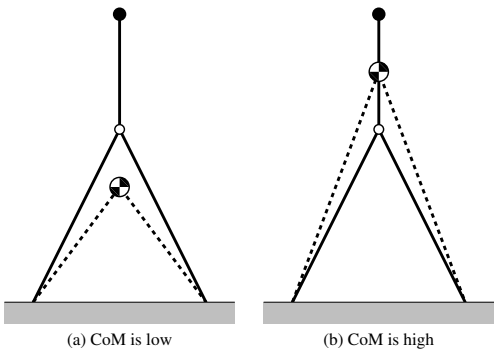

(a) CoM is low (b) CoM is high

Fig. 5. Comparison of two models with high and low CoM positions

IV. ASYMPTOTIC STABILITY OF DYNAMIC GAIT

A. Constraint on restored mechanical energy

The $i+1$-th kinetic energy just before impact is determined by the i-th one and the restored mechanical energy in the i-th step; it is expressed as

$$K^-[i+1] = K^+[i] + \Delta E. \tag{23}$$

Here, by considering the relation

$$\varepsilon = \frac{K^+[i]}{K^-[i]}, \tag{24}$$

we obtain the following recurrence formula for K^-:

$$K^-[i+1] = \varepsilon K^-[i] + \Delta E. \tag{25}$$

If ε and ΔE are kept constant, the general term of K^- is obtained as

$$K^-[i] = \frac{\Delta E}{1-\varepsilon} + \varepsilon^i \left(K^-[0] - \frac{\Delta E}{1-\varepsilon} \right), \tag{26}$$

and we get

$$K^-[\infty] = \lim_{i\to\infty} K^-[i] = \frac{\Delta E}{1-\varepsilon}. \tag{27}$$

This proves asymptotic stability. Let $\dot{\theta}_*^- = \dot{\theta}_1^- = \dot{\theta}_2^- > 0$ be the equilibrium point of the angular velocity just before impact in the forward walking motion, and it should satisfy

$$K^-[\infty] = \frac{1}{2}\bar{M}^- \left(\dot{\theta}_*^-\right)^2 = \frac{\Delta E}{1-\varepsilon}. \tag{28}$$

This leads to the following result.

$$\dot{\theta}_*^- = \sqrt{\frac{2\Delta E}{\bar{M}^-(1-\varepsilon)}} \tag{29}$$

This stability mechanism is equivalent to that of a rimless wheel [4], and the generated gait always becomes asymptotically stable so long as collisions occur.

B. Without constraint on restored mechanical energy

We next consider a case without a constraint on the restored mechanical energy. ΔE should be considered to be a discrete state variable, $\Delta E[i]$, and the recurrence formula should be rewritten as

$$K^-[i+1] = \varepsilon K^-[i] + \Delta E[i]. \tag{30}$$

For two given initial kinetic energies, $K_1^-[i]$ and $K_2^-[i]$, the following equations

$$K_1^-[i+1] = \varepsilon K_1^-[i] + \Delta E_1[i], \tag{31}$$

$$K_2^-[i+1] = \varepsilon K_2^-[i] + \Delta E_2[i], \tag{32}$$

hold and define the approximate rate of change of the return map:

$$\delta := \frac{K_1^-[i+1] - K_2^-[i+1]}{K_1^-[i] - K_2^-[i]}. \tag{33}$$

The asymptotic stability condition is then expressed as

$$|\delta| < 1. \tag{34}$$

Figs. 6 and 7 plot the Poincaré return map of K^- for three values of l_T and m_T. We can conclude from their slopes that all gaits are asymptotically stable around each equilibrium point. The slopes are mainly determined by the energy loss coefficient, i.e., the impact posture. The slope becomes ε for $\Delta E = 0$, but differs if there is no constraint on the restored mechanical energy. We discuss this in the next section.

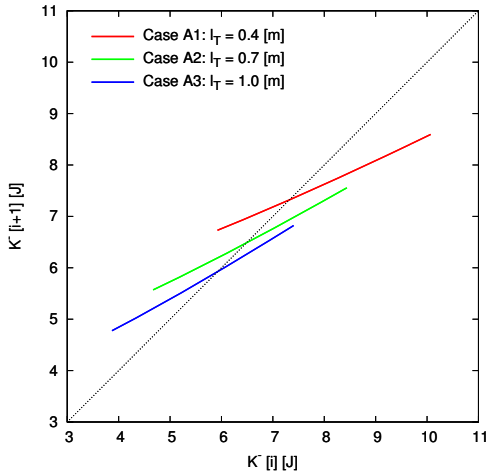

Fig. 6. Poincaré return map of kinetic energy just before impact for three values of l_T

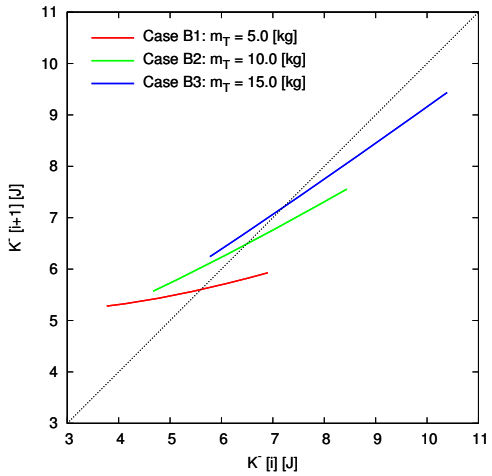

Fig. 7. Poincaré return map of kinetic energy just before impact for three values of m_T

V. ENERGY FEEDBACK STRUCTURE IN DYNAMIC WALKING SYSTEMS

A. Mechanism of discrete energy feedback

As seen in Figs. 6 and 7, the Poincaré return maps of K^- seem to be straight lines. This result implies that the relation between $K^-[i]$ and $\Delta E[i]$ also should be linear. Figs. 8 and 9 plot the relations, and we can see that they are almost straight in all cases. They should be able to be approximated by linear functions of the form

$$\Delta E[i] = C_1 K^-[i] + C_0, \tag{35}$$

where C_1 and C_0 are constant coefficients. By substituting this into Eq. (30), we obtain

$$K^-[i+1] = (\varepsilon + C_1)K^-[i] + C_0, \tag{36}$$

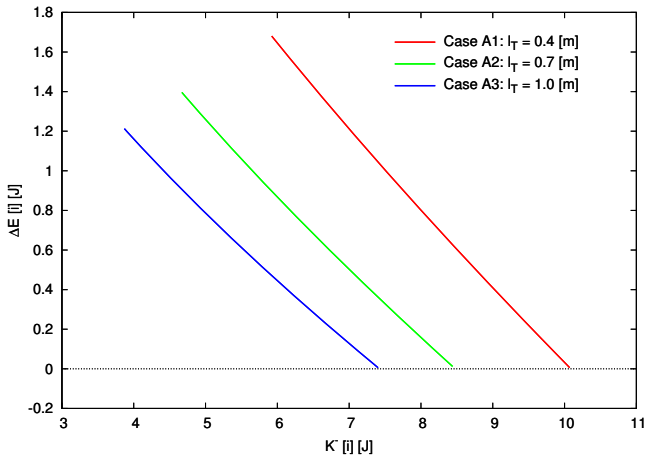

Fig. 8. $K^-[i]$ versus $\Delta E[i]$ for three values of l_T

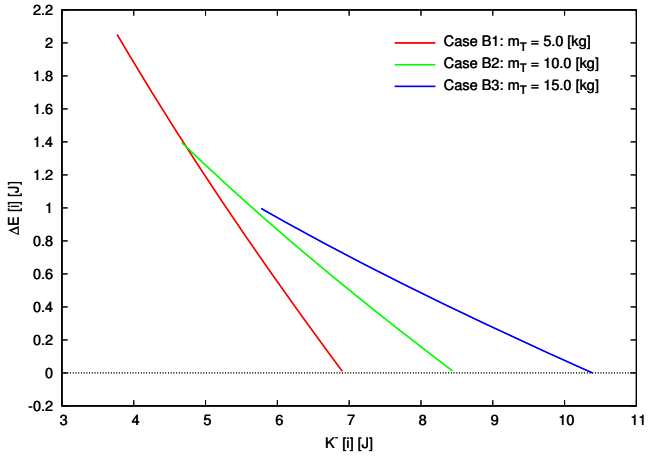

Fig. 9. $K^-[i]$ versus $\Delta E[i]$ for three values of m_T

and the general term becomes

$$K^-[i] = (\varepsilon + C_1)^i \left(K^-[0] - \frac{C_0}{1-\varepsilon-C_1} \right) + \frac{C_0}{1-\varepsilon-C_1}. \tag{37}$$

The asymptotic stability is thus

$$K^-[\infty] = \lim_{i\to\infty} K^-[i] = \frac{C_0}{1-\varepsilon-C_1}. \tag{38}$$

Here, we assume the following condition holds.

$$|\varepsilon + C_1| < 1. \tag{39}$$

This stability principle can be shown to be the same as Eq. (25) by replacing $\varepsilon+C_1$ and C_0 with ε and ΔE, respectively.

It is remarkable that the restored mechanical energy in the form of Eq. (35) can be regarded as a state feedback control for the discrete walking system of Eq. (30). Fig. 10 shows the block diagram. The coefficient C_0 is the feed-forward input and $K^-[i]$ is the system's state. It is known that passive dynamic walking inherently has a feedback stabilization mechanism [10], whereas a similar mechanical energy mechanism exists in dynamic walking system with a constraint on impact posture.

We calculated the values of the coefficients in the numerical examples. Tables II and III lists these coefficients calculated by the least squares method and limit value of K^-. They show that Eq. (39) is satisfied for all cases.

TABLE II

MEASURED COEFFICIENTS AND $K^-[\infty]$ FOR THREE l_T CASES

	Case A1	Case A2	Case A3
l_T [m]	0.4	0.7	1.0
ε	0.8527	0.8938	0.9207
C_1	−0.4031	−0.3664	−0.3410
C_0	4.0397	3.0783	2.5027
$\varepsilon + C_1$	0.4496	0.5273	0.5796
$K^-[\infty] = C_0/(1-\varepsilon-C_1)$	7.3399	6.5126	5.9539

TABLE III

MEASURED COEFFICIENTS AND $K^-[\infty]$ FOR THREE m_T CASES

	Case B1	Case B2	Case B3
m_T [kg]	5.0	10.0	15.0
ε	0.8571	0.8938	0.9082
C_1	−0.6500	−0.3664	−0.2155
C_0	4.4593	3.0783	2.2197
$\varepsilon + C_1$	0.2072	0.5273	0.6927
$K^-[\infty] = C_0/(1-\varepsilon-C_1)$	5.6246	6.5126	7.2222

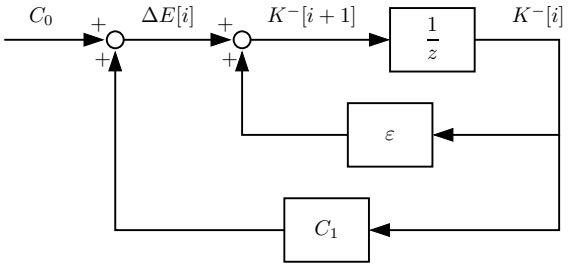

Fig. 10. Energy feedback structure in discrete-time walking system

B. Detection limit of limit-cycle stability

Here we discuss the detection limit of the limit cycle stability. Goswami *et al.* discovered that passive-dynamic walkers often exhibit period-doubling bifurcations and chaotic behavior [9]. The active walker this paper considers also exhibits bifurcations. When $l_T = 0$ and $T_{\rm set}$ is large, ε approaches -1. Fig. 11 shows the Poincaré return map of K^- for three values of $T_{\rm set}$, and Table IV lists the calculated coefficients and the limit value of K^-. From Fig. 11, we can see that ε almost becomes -1 when $T_{\rm set} = 1.485$ [s], and the calculated result in this case shows that the gait is unstable. In contrast, the numerical simulation indicates that the limit cycle converges to a stable 2-period gait, as shown in Fig. 12. This means the stability detection using an approximate linear function was an error. This is because the linear function can only find a stable 1-period gait or unstable gait.

For this reason, we must check the features of $\Delta E[i]$ with respect to $K^-[i]$ in the whole range to understand the limit cycle stability exactly. We must conclude that it is impossible to detect the stability of 2^n-period gaits. As shown in Fig. 13, a linear approximation of the Poincaré return map can only give detections of stability or instability about the generated dynamic gait. Therefore, to clarify not the local but the global stability of the dynamic gait, the restored mechanical energy

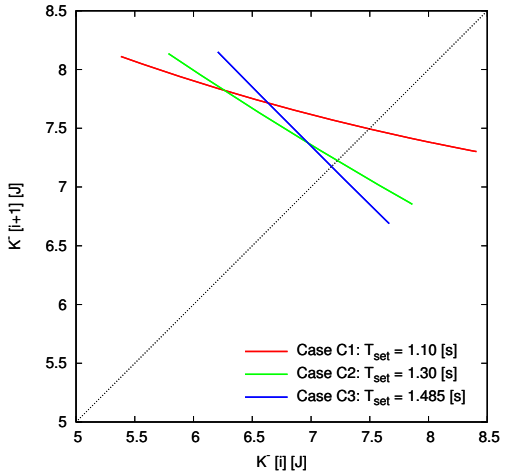

Fig. 11. Poincaré return map of kinetic energy just before impact for three values of $T_{\rm set}$

TABLE IV

MEASURED COEFFICIENTS AND $K^-[\infty]$ FOR THREE $T_{\rm set}$ CASES

	Case C1	Case C2	Case C3
$T_{\rm set}$ [s]	1.10	1.30	1.485
ε	0.8727	0.8727	0.8727
C_1	−1.1402	−1.4909	−1.8747
C_0	9.5085	11.6941	14.3630
$\varepsilon + C_1$	−0.2674	−0.6181	−1.0019
$K^-[\infty] = C_0/(1-\varepsilon-C_1)$	7.5022	7.2270	Unstable

should obey the following nonlinear function

$$\Delta E[i] = \sum_{j=0}^{\infty} C_j \left(K^-[i]\right)^j . \qquad (40)$$

However, the stability analysis becomes complicated in this case.

VI. CONCLUSION AND FUTURE WORK

In this paper, we investigated the asymptotic stability of dynamic bipedal gaits that have a constraint on the impact posture only and discussed the energy feedback structure. We showed that there is a limit to detecting the limit cycle stability including 2^n-period gaits with a linear function approximation of the return map.

As discussed in [4], two constraint conditions are necessary to guarantee limit cycle stability, and in this sense, dynamic walkers should have enough active joints to meet them. We conclude that all or almost all joints of the robot must be driven during the stance phase to realize stable dynamic walking.

In the future, we will investigate the limit cycle stability in a more general case without any constraint conditions.

VII. ACKNOWLEDGMENTS

This work was partially supported by a Grant-in-Aid for Scientific Research, (B) No. 18360115, provided by the Japan Society for the Promotion of Science (JSPS).

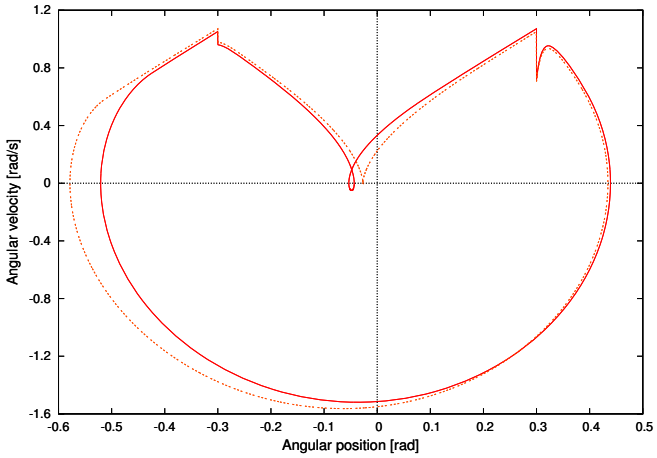

Fig. 12. Phase plane of 2-period gait where $T_{\rm set} = 1.485$ [s]

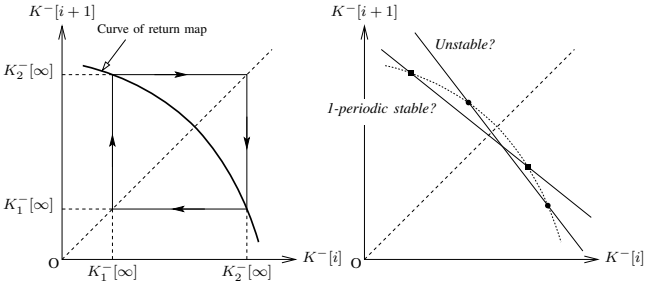

(a) Stable 2-period case (b) Examples of error detection

Fig. 13. Stable 2-period gait and error detection examples

REFERENCES

[1] T. McGeer, "Passive dynamic walking," *Int. J. of Robotics Research*, Vol. 9, No. 2, pp. 62–82, 1990.

[2] S. Hosoe, K. Takeichi, S. Kumai and M. Ito, "Analysis of stability of dynamic biped locomotion with high gain feedback," *Trans. of the Society of Instrument and Control Engineers*, Vol. 22, No. 9, pp. 948–954, 1986. (In Japanese)

[3] J. W. Grizzle, G. Abba and F. Plestan, "Asymptotically stable walking for biped robots: Analysis via systems with impulse effects," *IEEE Trans. on Automatic Control*, Vol. 46, No. 1, pp. 51–64, 2001.

[4] F. Asano and Z.W. Luo, "Asymptotically stable gait generation for biped robot based on mechanical energy balance," *Proc. of the IEEE/RSJ Int. Conf. on Intelligent Robots and Systems*, pp. 3327–3333, 2007.

[5] M. Wisse, D. G. E. Hobbelen and A. L. Schwab: "Adding an upper body to passive dynamic walking robots by means of a bisecting hip mechanism," *IEEE Transactions on Robotics*, Vol. 23, No. 1, pp. 112–123, 2007.

[6] F. Asano and Z.W. Luo, "Dynamic analyses of underactuated virtual passive dynamic walking," *Proc. of the IEEE Int. Conf. on Robotics and Automation*, pp. 3210–3217, 2007.

[7] F. Asano and Z.W. Luo, "The effect of semicircular feet on energy dissipation by heel-strike in dynamic biped locomotion," *Proc. of the IEEE Int. Conf. on Robotics and Automation*, pp. 3976–3981, 2007.

[8] F. Asano and Z.W. Luo, "Underactuated virtual passive dynamic walking with an upper body," *to appear in Proc. of the IEEE ICRA2008*.

[9] A. Goswami, B. Thuilot and B. Espiau, "Compass-like biped robot Part I: Stability and bifurcation of passive gaits," *INRIA Research Report*, No. 2996, 1996.

[10] Y. Sugimoto and K. Osuka, "Stability analysis of passive dynamic walking – An approach via interpretation of Poincare map's structure," *Trans. of ISCIE*, Vol. 18, No. 7, pp. 255–260, 2005. (In Japanese)